Published as: Materials & Design 146 (2018) 96-107

In situ DSC investigation into the kinetics and microstructure of dispersoid formation in Al-Mn-Fe-Si(-Mg) alloys

Richard H. Kemsies[a)], Benjamin Milkereit[a),b),*], Sigurd Wenner[c)], Randi Holmestad[c)], Olaf Kessler[a),b)]

a) Chair of Materials Science, Faculty of Mechanical Engineering and Marine Technology, University of Rostock, Albert-Einstein-Str. 2, 18059 Rostock, Germany

b) Competence Center °CALOR, Department Life, Light & Matter, Faculty of Interdisciplinary Research, University of Rostock, Albert-Einstein-Str. 25, 18059 Rostock, Germany

c) Department of Physics, NTNU, Høgskoleringen 5, 7491 Trondheim, Norway

* Corresponding author at: Chair of Materials Science, Faculty of Mechanical Engineering and Marine Technology, University of Rostock, Albert-Einstein-Str. 2, 18059 Rostock, Germany. *E-mail address: benjamin.milkereit@uni-rostock.de* (B. Milkereit).

Graphical abstract

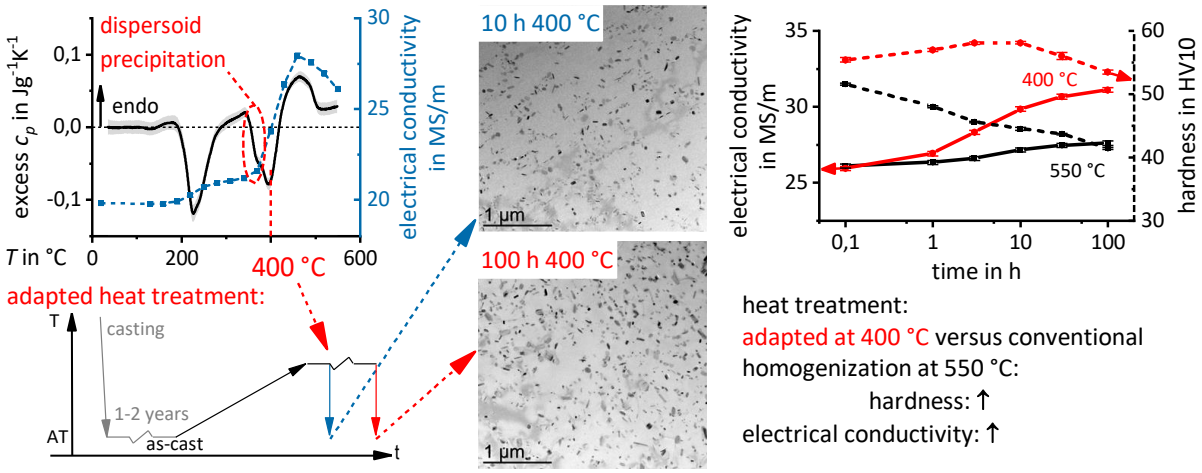

Highlights

- The dependence of dispersoid precipitation on temperature and heating rate was analyzed by various techniques.
- Adapting the homogenization process causes dispersoid strengthening by Mn-rich dispersoids in Al-Mn-Fe-Si(-Mg) alloys.
- Significant increases in hardness (30%) and electrical conductivity (10%) compared to standard homogenization were obtained.
- The achieved properties make these alloys attractive for electrical conductors operating in environments of up to 140 °C.

Abstract
Dispersoid strengthening in Al-Mn-Fe-Si(-Mg) aluminum wrought alloys can play an important role in applications at elevated temperatures. Fine and evenly distributed dispersoids are needed to increase alloy strength, which can be achieved by conducting an adapted homogenization heat treatment. In this work for the first time, the precipitation behavior of dispersoids in direct chill casted Al-Mn-Fe-Si(-Mg) alloys was systematically investigated in situ during heating by means of differential scanning calorimetry. In situ analysis of the phase transformation kinetics during heating and homogenization was complemented by ex situ testing of the electrical conductivity and Vickers hardness, as well as micro- and nano-structural analyses by optical light and transmission electron microscopy. The influence of the heating rate on precipitation behavior was determined by calorimetric in situ experiments, covering a wide heating rate, ranging from 0.003 to 2 K/s. The influence of 400 and 550 °C homogenization temperatures and soaking durations on hardness and electrical conductivity was also investigated. The highest dispersoid strengthening was obtained after heat treating the as-cast Mg-containing alloy at 400 °C for 3 to 10 h. Furthermore, the Mg content heavily influenced the precipitation behavior by forming β-Mg2Si precursor phases, which can act as nucleation sites for dispersoid precipitation.

Keywords
EN AW-3105, dispersoids, homogenization, DSC, TEM, electrical conductivity

1. Introduction

The first heat treatment after casting is an important step in the manufacturing process of Al-Mn-Fe-Si(-Mg) wrought alloys. This step, known as homogenization, should ensure that the alloy possesses homogeneous material properties and can undergo further processing with ease. Homogenization includes the globular shaping of primary phases, the reduction of segregations, and the precipitation of dispersoids. The evolution of microstructures during the homogenization process of Al-Mn-Fe-Si(-Mg) alloys has thus been widely reported, with numerous studies on the transformation of primary phases [1–7] and the precipitation behavior of dispersoids [1,6,8–14].

The term dispersoids in Al-Mn-Fe-Si(-Mg) alloys mostly describes the nanoscale intermetallic particles that precipitate from the supersaturated as-cast state during the first heating. Depending on the total amount of Si in Al-Mn-Fe-Si alloys, the dispersoids usually consist of the plate-shaped Al_6(Mn,Fe) phase [15] for low-Si alloys or the cubic α-Al(Fe,Mn)-Si phase [9] for high-Si alloys. Mn remains in solid solution after the casting process, forming a supersaturated solid solution. The total amount of Mn in solid solution seems to be relatively unaffected by the solidification rate [16]. The dispersoid precipitation starts during heating at a temperature of ~350 °C [6,8,14]. Continued heating initially causes both the particle diameter and number density to increase with temperature. However, above ~400 °C, the number density decreases while the diameter increases [8].

Small amounts of Mg and Cu are frequently added to Al-Mn-Fe-Si(-Mg) alloys to enhance their mechanical properties. If the concentration of these elements is high enough, it enables the precipitation of an Mg-Si(-Cu) sequence of precursors and equilibrium phases. The Mg-Si(-Cu) sequence and their influence on the mechanical properties has been previously investigated [17]. The precipitation of dispersoids is correlated with those Mg-Si(-Cu) phases.

Lodgaard and Ryum [14] have observed an additional 'u-phase' that forms through Mn and Fe diffusion into the precursor β′-Mg_2Si phase at ~350 °C. A further increase in temperature causes the dispersoids to precipitate along this 'u-phase'. This might lead to a heterogeneous but fine distribution of dispersoids.

A fine and even distribution of dispersoids can be used to hinder recrystallization [12] and enhance the mechanical properties for high-temperature applications, such as electrical conductors operating at temperatures of up to 140 °C [18]. Furthermore, the sufficient number density and particle diameter of the dispersoids means that they can also improve the strength of Al-Mn-Fe-Si(-Mg) alloys by dislocation pinning [9,19–21]. However, an increase in strength due to dispersoids can only be achieved by adapting the homogenization treatment parameters, which usually consist of a heat treatment for several hours at high temperatures in the 550–580 °C range. Muggerud et al. [19] investigated four as-cast Al-Mn-Fe-Si alloys with various Mn and Si concentrations, where they performed hardness and tensile tests after heating (at 50 K/h) to 375 and 450 °C, respectively, with various annealing times. Their tensile tests demonstrated that the yield strength was highest in the alloys that underwent a heat treatment at 375 °C for 24 h.

Most investigations of dispersoid formation have been conducted as ex situ experiments. Thermoelectric power (TEP) [22], electrical conductivity (EC) measurements [8], and microscopy at different scales (mostly scanning electron microscope (SEM) and transmission electron microscopy (TEM)) are the common observations made during these investigations. Only a few in situ investigations of dispersoid formation exist to date, with the observations acquired from diffraction experiments consisting of synchrotron radiation and EC measurements [6].

Differential scanning calorimetry (DSC) is a well-established method for the in situ analysis of secondary phase precipitation and dissolution in alloys, such as 2xxx, 6xxx, and 7xxx alloys [23]. However, an exhaustive literature search found no documented evidence regarding the application of DSC for the in situ analysis of dispersoid formation. Among other factors, this is likely due to problems in the evaluation of DSC experiments. Previous DSC investigations of Al-Mg-Si(-Mn) alloys generally assumed that all dissolution reactions ended with complete dissolution of the Mg_2Si phase. This assumption makes it possible to apply a zero-level polynomial curve correction to the assumed reaction free regions [23]. However, the present results will show that even at high temperatures (up to 600 °C), reactions might occur in the form of the dissolution and growth of Mn-containing dispersoids. It is therefore necessary to develop a new evaluation routine to depict the complete dispersoid reactions, which has been accomplished in this paper. In situ DSC results of the dispersoid precipitation in Direct Chill (DC) casted Al-Mn-Fe-Si(-Mg) alloys, along with a complementary micro- and nanostructural analysis, are presented here.

2. Materials and Methods

2.1. Materials and heat treatments

Two Al-Mn-Fe-Si(-Mg) alloys based on the standard EN AW-3105 were investigated. The influence of Mg-Si precursors was analyzed by producing one alloy with 0.6 wt% Mg and one alloy without almost any Mg. The material was DC-cast to Ø 80 mm × 2000 mm ingots. The chemical composition and electrical conductivity of the as-cast states are given in Table 1.

Two different time-temperature programs were performed to determine the parameters that will yield the optimal alloy strength (Fig. 1). A linear heating program was first conducted to investigate the heating process and the precipitation kinetics of the dispersoids, where the heating rates were varied from 0.003 to 2 K/s (Fig. 1a). A non-linear heat treatment was then performed to simulate the typical heating of Al-Mn-Fe-Si(-Mg) alloys in industrial furnaces, as follows: 20 °C to 290 °C at 0.03 K/s, 290 °C to 350 °C at 0.012 K/s, 350 °C to 390 °C at 0.0056 K/s and 390 °C to 400 °C at 0.0028 K/s (Fig. 1a). This temperature profile was based on the measured temperature profile of a cast billet. The influence on the precipitation behavior of certain defined previous heat treatments of the as-cast samples was also analyzed by DSC reheating (Fig. 1b).

During the interrupted heating process, samples were linearly heated at 0.01 K/s in a dilatometer Baehr DIL 805A/D to the dedicated temperature of a given experiment and then gas quenched to ambient temperature. Isothermal soaking was performed in an air furnace Carbolite CWF 1100. After reaching the dedicated soaking duration of a given experiment, the samples were then water quenched to ambient temperature.

alloy	mass fraction in %						EC
	Si	Fe	Cu	Mn	Mg	Cr	in MS/m
EN AW-3105 without Mg	0.5	0.38	0.142	0.71	0.0007	0.006	21.5 ± 0.1
EN AW-3105	0.48	0.38	0.145	0.7	0.6	0.001	19.8 ± 0.1
EN 573-3	< 0.6	< 0.7	< 0.3	0.3-0.8	0.2-0.8	< 0.2	

Table 1. Mass fraction of alloying elements and as-cast electrical conductivity (EC) of the investigated alloys as well as the composition range according to EN 573-3.

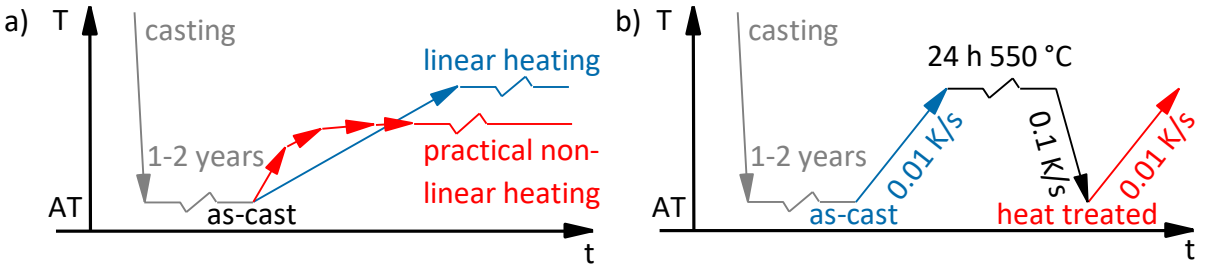

Fig. 1. Time-temperature programs for a) DSC, electrical conductivity measurements and microstructural investigations, and b) DSC reheating measurements.

2.2. Precipitation kinetic analysis by DSC

The in situ DSC investigations were conducted and evaluated by adapting and improving the procedure described by Osten et al. [23]. Two different DSC devices were combined to cover a wide range of heating rates: slow heating rates (0.003 K/s to 0.1 K/s) were conducted with a Setaram Sensys or 121 DSC device, and faster heating rates (0.3 K/s to 2 K/s) were conducted with a PerkinElmer DSC 8500 device. The DSC samples were machined to Ø 6 mm × 21.65 mm (Setaram) and Ø 6.2 mm × 1 mm (PerkinElmer), respectively. High purity aluminum samples of the same dimensions were used as references in the experiments. To balance the sample and reference furnace, the masses of all samples and references were adapted to $\Delta m < 0.1\%$ by carefully grinding the samples with abrasive paper. All samples (including the reference samples) were covered with standard aluminum crucibles. Despite ensuring that the greatest care was taken in conducting the experiments, the resulting DSC curves still possessed a certain unavoidable degree of scattering within a series of samples at the same heating rate, likely due to slight differences in sample positioning within the sensor or slight sensor-lid position variations. Osten et al. [23] proposed a zero-level polynomial fit correction to reduce the remaining curvature. However, this requires reaction-free zones to allow proper fitting of the polynomial. Here, due to the lack of reaction-free zones at high temperatures (because the dissolution of dispersoids occurs), a new evaluation approach was applied.

This new evaluation assumes that a major component of the observed DSC curve fluctuations is related to reasons that are specific to a given DSC run. Applying the same heating rate over a series of DSC run will yield DSC curves that are randomly scattered around a true average value. Therefore, the true average value of the DSC curve can be determined if a sufficient number of repetition experiments are conducted. However, correct interpretation of the results requires a sound understanding of the various factors that may introduce scatter to the DSC curve, such as:

1. the noise of the measurement signal;
2. differences in the measurement setup due to:
    a. slight changes to the sample positions in the DSC measuring cell (and of the furnace cover in the PerkinElmer device);
    b. changes in the devices (e.g., icing, ambient temperature, coolant temperature);
    c. slight variations in the sample masses; and
3. material inhomogeneities (e.g. macro segregations). The as-cast material may possess variable local element concentrations, which may lead to differences in both the absolute heat capacity C_p and the intensities of the reactions.

alloy	heating rate in K/s	number of experiments
EN AW-3105 with Mg	0.003	1
	0.01 … 2	6
EN AW-3105 without Mg	0.003	1
	0.01 … 0.1	2
	0.3 … 2	6

Table 2. Conducted DSC experiments for each heating rate.

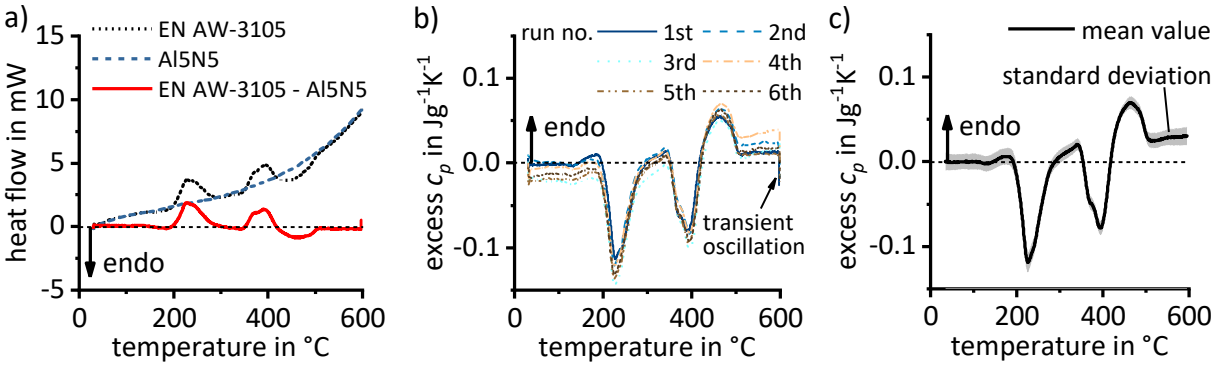

Fig. 2. Data processing of a DSC heating curve (0.01 K/s) of as-cast EN AW-3105. The data processing consists of: a) subtracting the sample heat flow curve (black) from the reference curve (blue), yielding the zero-level heat flow curve (red); b) dividing the zero-level heat flow curve by the sample mass and heating rate to obtain the excess cp value (shown for six experiments here); and c) calculating mean and standard deviation (shaded gray area) of the excess cp from several individual measurements. The black dashed line on each plot marks the zero-level values of each dataset, and the black arrow marks the zone dominated by endothermic reactions.

It is therefore important to accurately capture the mean and standard deviation for each set of experiments. The following data processing routine was conducted for all DSC measurements, and is illustrated in Fig. 2. First, the heat flow curve for each sample was subtracted from the reference measurement to yield the zero-level heat flow curve for each sample (Fig. 2a). These zero-level heat flow curves were then divided by the sample mass and heating rate to obtain the excess c_p values [23] (Fig. 2b). Finally, the mean value was calculated from all the existing excess c_p values for a given heating rate. The standard deviation was calculated when there were at least six measurements for a given heating rate (Fig. 2c). The range (maximum value minus minimum value) was calculated when there were fewer than six measurements. It should be noted that both the standard deviation and range increased when the heating rates were close to the lower scan rate limit of the DSC device, which is caused by the lower measurement signal-to-noise ratio and longer times between single experiments. The number of experiments for each heating rate is shown in Table 2. Although the masses of the samples and references were nearly identical, a vertical shift was applied to all the excess c_p curves. This was the result of varying absolute C_p values between the samples, as, and also between a given sample and the reference. The different c_p values for a given sample and the reference were corrected by shifting the very beginning (directly behind the transient oscillation of the measurement signal [23]) of the mean value curve to zero. The different c_p values of the samples at one temperature are probably due to macro segregations, causing the increased range and standard deviation at the very beginning of the curve. This evaluation proved that there was good reproducibility of the DSC results, and also illustrated the ongoing endothermic dissolution reaction up to 600 °C.

2.3. Micro- and Nanostructure analysis

Optical light microscopy (OLM) and TEM investigations were undertaken to analyze the structural properties of the samples after they underwent the heat treatments depicted in Fig. 1. OLM samples were embedded in epoxy, grinded, and polished according to standard preparation methods, and then etched with a 10% H_2PO_4 solution for at least 10 s to enhance

the contrast of the dispersoids. Images were acquired on a Leica DMI5000 M microscope. TEM samples were cut to Ø 3 mm × 1 mm discs, ground to foils (~100 µm thickness), and electropolished with a Struers TenuPol-5 using an electrolytic solution consisting of 1/3 nitric acid and 2/3 methanol. The applied voltage was 20 V and the electrolyte temperature was -25 °C. Bright-field images were acquired on a Philips CM30, operated at 150 kV, and a Gatan PEELS (parallel electron energy loss spectroscopy) system was used to obtain thickness measurements at the imaged areas. STEM-EDS (energy dispersive x-ray spectroscopy) elemental mapping was performed on a JEOL JEM-2100F, operated at 200 kV, with an Oxford EDS silicon drift detector. Elemental maps were constructed by integrating the characteristic Kα-peaks. Quantitative results of the dispersoids were determined by employing the ImageJ image analyzer software to evaluate at least four TEM images, with each covering an area of about ~11 µm^2. The volume density of the dispersoids was calculated by dividing the counted dispersoids of the investigated area with the PEELS measured thickness of that area. The size distribution of the dispersoids was evaluated by the mean Feret diameter (maximum caliper) [24]. SEM-EDS was performed on a Zeiss Merlin VP compact, operated at 20 kV, with a Bruker Quantax EDS detector. Elemental analysis was conducted by evaluating the characteristic Kα-peaks.

EC measurements were conducted using a Sigmascope SMP1A Eddy current device with a probe diameter of 14 mm and a testing frequency of 60 kHz. Samples were machined to Ø 15 mm × 2 mm and heat treated in an air furnace Carbolite CWF 1100 according to Fig. 1. The samples were subsequently water quenched to ambient temperature at specific temperatures and soaking durations throughout the homogenization process. To eliminate the effect of a fluctuating ambient temperature, a non-heat treated sample was measured as the reference after each measurement. The results were thus normalized to the actual temperature.

Vickers hardness tests were performed on the samples used for EC measurements according to ISO 6507-1. A hardness tester Wolpert Diatronic 2 RC was used, with a testing load of 98.067 N (HV10). Each hardness value reported is an average value based on six indentations made on each sample.

3. Results and discussion

3.1. Precipitation during linear heating – DSC and EC

Fig. 3 shows in situ DSC and ex situ EC measurements of EN AW-3105 with and without Mg during heating from the initial as-cast state and re-heating after conventional homogenization at 550 °C for 24 h. In addition to the excess c_p curves, the related zero-level is plotted. Excess c_p values exceeding this zero-level (i.e., positive c_p values) indicate the dominance of endothermic dissolution reactions. However, DSC only measures the sum of any heat effects, such that peaks within a DSC curve do not necessarily have to be equal to the underlying microstructural reaction and its own intensity maximum. In contrast, EC strongly depends on the individual alloying elements, and yields details on both the amount and sort of alloying elements in solid solution. EC measurements may thus aid in differentiating between the occurring reactions in the DSC signals. The identified phases that occurred during heating are listed in Table 3 and marked on the associated peaks in Fig. 3.

The excess c_p curves during heating from the as-cast, as well as from the homogenized state of EN AW-3105 with Mg, are dominated by a sequence of different precipitation and dissolution reactions. These reactions correspond well with the reactions of Al-Mg-Si(-Cu) (6xxx) alloys, which are produced by a sequence of metastable Mg-Si(-Cu)-phases and stable β-Mg_2Si and/or MgSiCu-phases [23]. It can be seen that the first exothermic reaction peak at ~200 °C, which is assigned to the precipitation of metastable Mg-Si(-Cu), corresponds well with the first slight increase in EC when the sample is heated from the as-cast state. This indicates that the precipitation of Mg-Si(-Cu) phases also have a small influence on EC. However, a larger EC increase of the initially as-cast EN AW-3105 with Mg can be seen in the 370–460 °C temperature range. According to Altenpohl [25], the most influential factors on EC in Al-Mn-Fe-Si(-Mg) alloys are the concentrations of Mn and Fe in solid solution. Therefore, the large increase in EC can be attributed to the decreasing Mn content in solid solution. This indicates precipitation of Mn-containing dispersoids. The EC maximum at ~460 °C is inferred to be the condition with the highest volume fraction of dispersoids [8,19]. The precipitation start temperature revealed by EC is ~370 °C. However, the DSC signal of the Mg-containing variant (initially as-cast) in this temperature region shows a peak g (β-Mg_2Si precipitation), which in detail has a shoulder (δ) at ~370 °C. The δ-peak-shoulder obviously corresponds well with the increase in EC, and can thus be attributed to the precipitation of Mn-containing dispersoids. In contrast, only a single peak without shoulder can be seen during heating from the conventionally homogenized state at ~400 °C. This shows that Mn is not in solution (or only in minimal amounts) after the conventional homogenization treatment. The low solubility of dispersoid-forming elements at the solution annealing and/or conventional homogenization temperature and the relatively slow Mn diffusion lead to the incomplete dissolution on Mn-containing dispersoids, even after soaking at 550 °C for 24 h. Nevertheless, DSC and EC confirm partial dissolution at higher temperatures. Above ~410 °C, the DSC signal is dominated by a large endothermic reaction that is frequently attributed to the dissolution of β-Mg_2Si [26]. However, in this case, an additional dissolution reaction is superimposed, with partial dissolution (Δ) and coarsening of the dispersoids via Ostwald ripening at temperatures above 500 °C [8]. This assumption is confirmed by the observed decrease in the EC signal at temperatures above 460 °C, indicating an increase in the Mn content in the solid solution.

peak	dissolution	precipitation
B	GP zones [27]	
d/e		β″ / MgSiCu precursor [27]
F	β″ / MgSiCu precursor	
δ		α-Al(Mn,Fe)Si [14]
g		β-Mg_2Si [26]
H	β-Mg_2Si	
Δ	α-Al(Mn,Fe)Si	

Table 3. Dissolution and precipitation peaks and the dedicated reactions in EN AW-3105. The peak variables refer to Fig. 3.

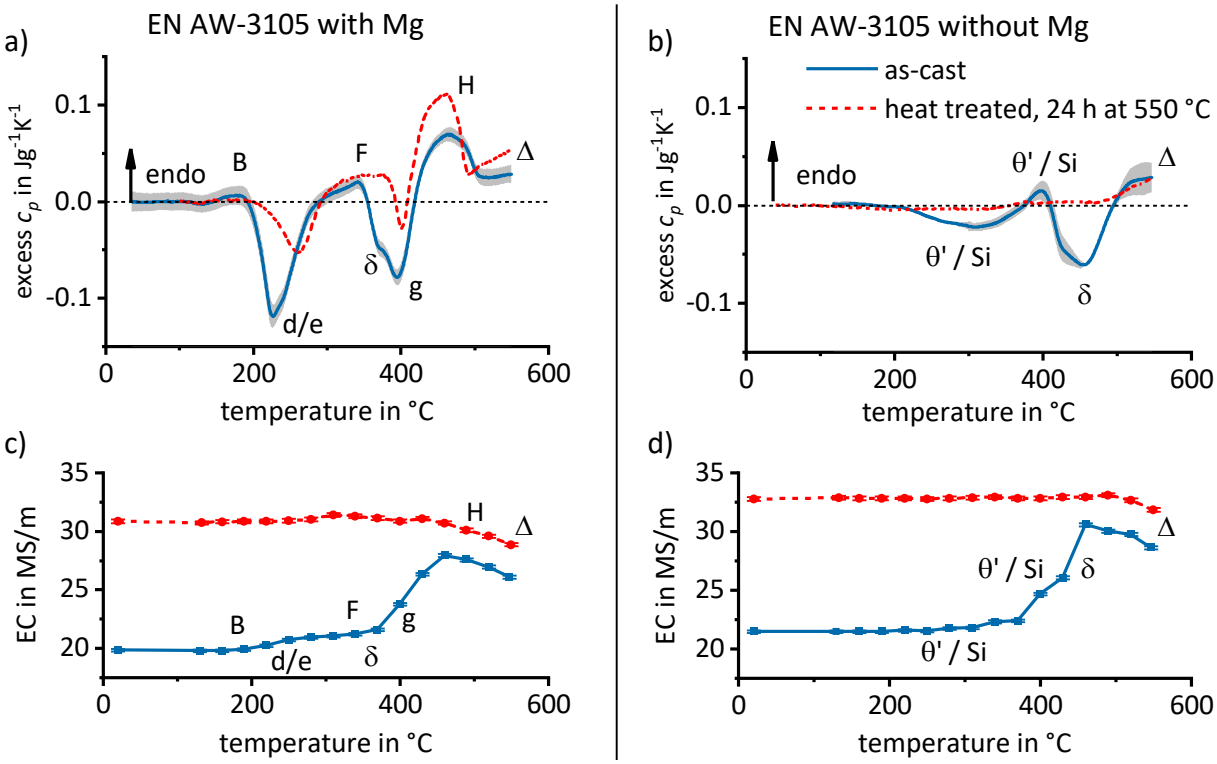

Fig. 3. In situ DSC (a, b) and ex situ electrical conductivity (EC) (c, d) heating curves (0.01 K/s) of as-cast and heat treated (24 h at 550 °C) EN AW-3105 with and without Mg. Precipitation reactions are marked as minuscule letters and dissolution reactions as capital letters (refer to Table 3 for further details).

The excess c_p signal during heating from the as-cast state of EN AW-3105 without Mg shows two exothermic reactions at ~300 °C and ~450 °C, and two endothermic reactions at ~400 °C and above 500 °C. The first exothermic peak is assigned to the precipitation of θ′ (Al_2Cu precursors) and diamond cubic Si particles (this will be discussed later with the TEM results). However, no increase in EC is observed during this precipitation reaction. The following endothermic peak at ~390 °C indicates the dissolution of these phases. The exothermic peak at ~450 °C is interpreted as the dispersoid precipitation reaction. However, it is interesting to note that a substantial increase in EC is already observed after heating to 370 °C. This EC increase is most likely caused by the dispersoid precipitation, which lowers the Mn concentration in solid solution. Similar to the Mg-containing alloy, the discrepancy between EC and DSC likely results from the overlapping heat flow signals, and are related to the dissolution of θ′/Si and the precipitation of dispersoids in this instance. It then becomes obvious that the θ′/Si dissolution must have a bigger specific enthalpy absorption compared to the enthalpy release of the Mn-containing dispersoid precipitation. Therefore, the dispersoid precipitation reaction might start at lower temperatures than can be observed in the DSC curve. However, the θ′/Si precipitation and dispersoid precipitation exothermic peaks can only be seen during the first heating from the as-cast state. Similarly, the EC remains constant during heating after 24 h at 550 °C, indicating the thermal stability of the dispersoids. The EC decreases and the DSC measurement shows an endothermic reaction signal (Δ) above 500 °C. This is likely due to dispersoid growth and dissolution by Ostwald ripening.

3.2. Precipitation during linear heating – Micro- and nano-structure analysis

Fig. 4 shows OLM images of EN AW-3105 with and without Mg, as-cast and after heating to dedicated temperatures. The as-cast microstructure of both alloys shows different phases that formed during the solidification process within the Al matrix. Most of these particles are Chinese script shaped, containing the elements Al, Fe, Mn, and Si (revealed by SEM-EDS; not shown here). They are probably primary particles of the α-Al(Mn,Fe)-Si phase. Other particles are also polygonal shaped in the Mg-containing alloy, containing the elements Mg, Si, Cu (revealed by SEM-EDS; not shown here), and in EN AW-3105 without Mg, consisting of Si only. After heating to 400 °C at a heating rate of 0.01 K/s, numerous Mg_2Si particles precipitated in the Mg-containing alloy, which corresponds well with the large exothermic reaction peak observed in the DSC experiment. The alloy without Mg was heated just over the first exothermic peak (310 °C) to identify the phases that precipitate between 220 °C and 380 °C. Some small particles precipitated inhomogeneously within the material, but these precipitates began to dissolve with further heating and completely vanished by 460 °C. It is assumed that this behavior corresponds to the endothermic reaction observed in the DSC experiments at ~400 °C.

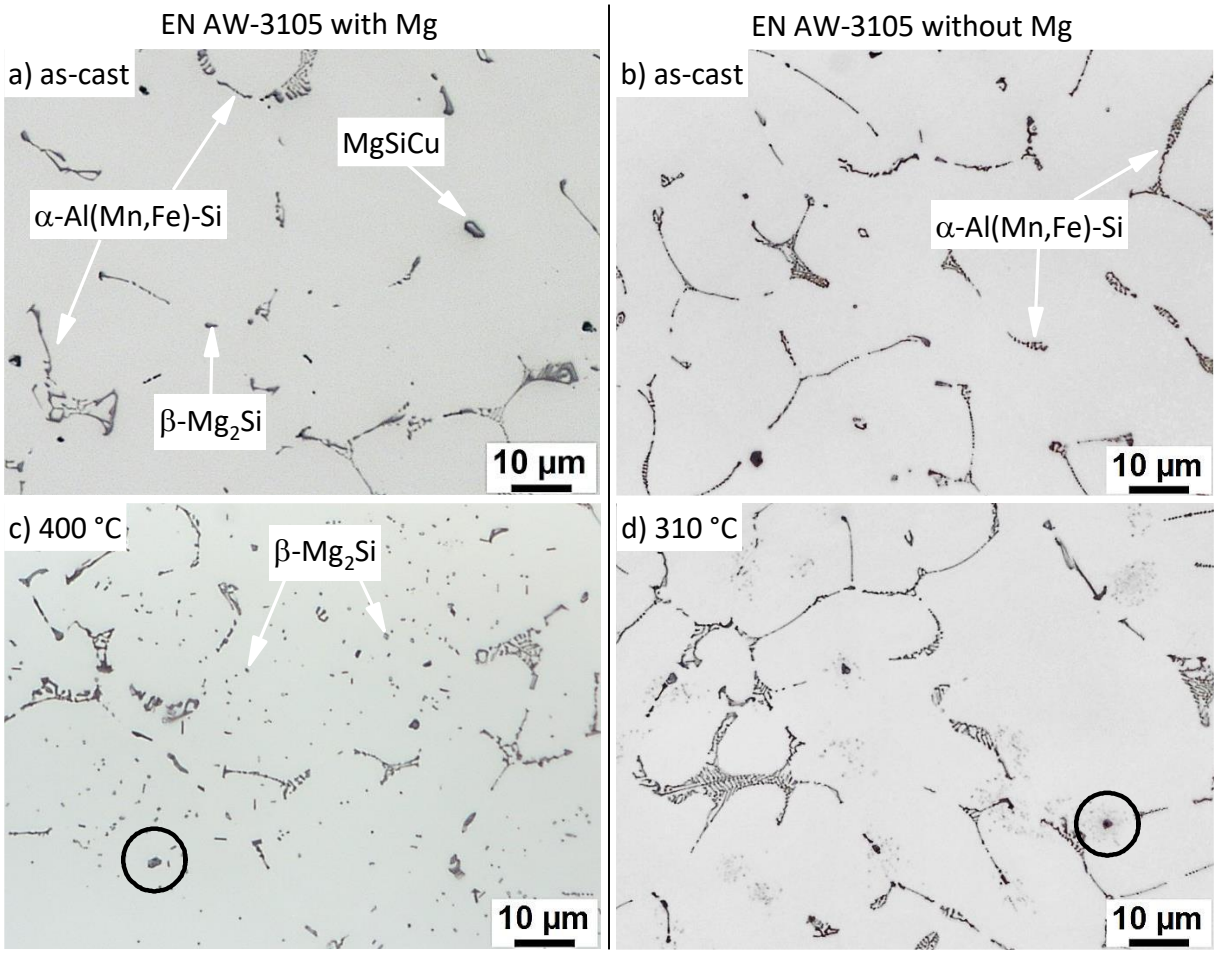

Fig. 4. OLM images of EN AW-3105 with (a,c) and without Mg (b,d), as-cast (a,b) and heated to dedicated temperatures (c: 400 °C; d: 310 °C) at 0.01 K/s and subsequently water quenched to ambient temperature. Circles highlight features that have been investigated by TEM (Fig. 5).

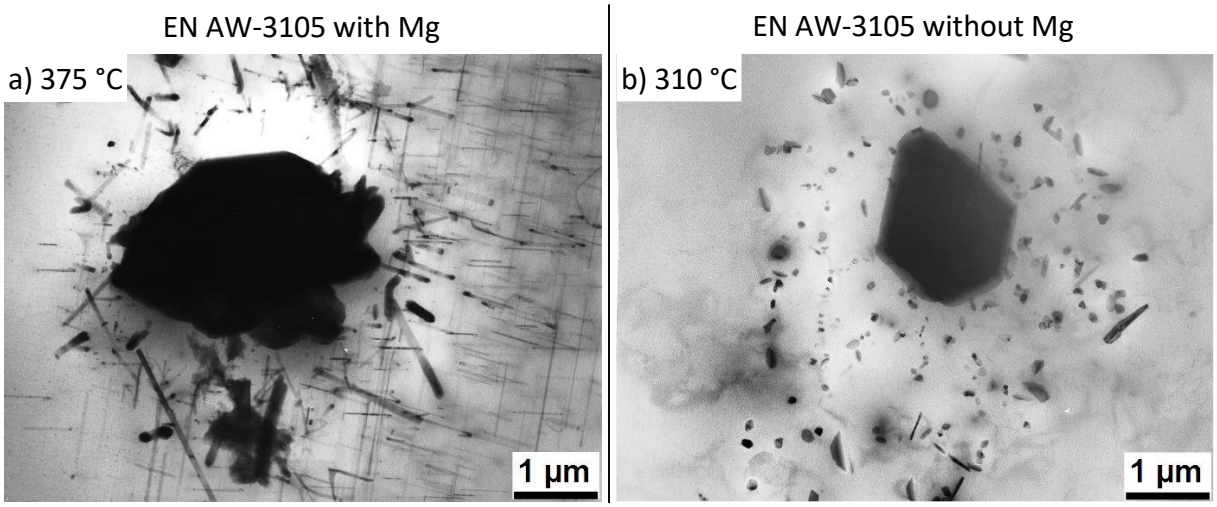

Fig. 5. TEM bright field images of EN AW-3105 with (a) and without Mg (b), heated to dedicated temperatures at 0.01 K/s and subsequently water quenched to ambient temperature. These images correspond to the circles that highlighted key features in Fig. 4.

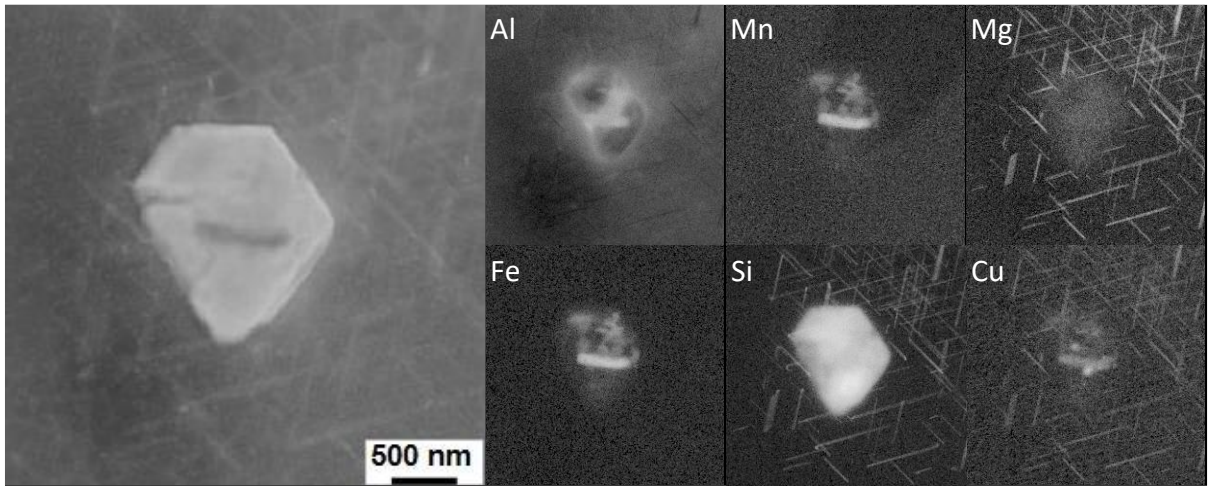

Fig. 6. STEM annular dark field images of the feature in Fig. 5a, and corresponding EDS maps of EN AW-3105 with Mg, heated to peak δ (375 °C) at 0.01 K/s and subsequently water quenched to ambient temperature.

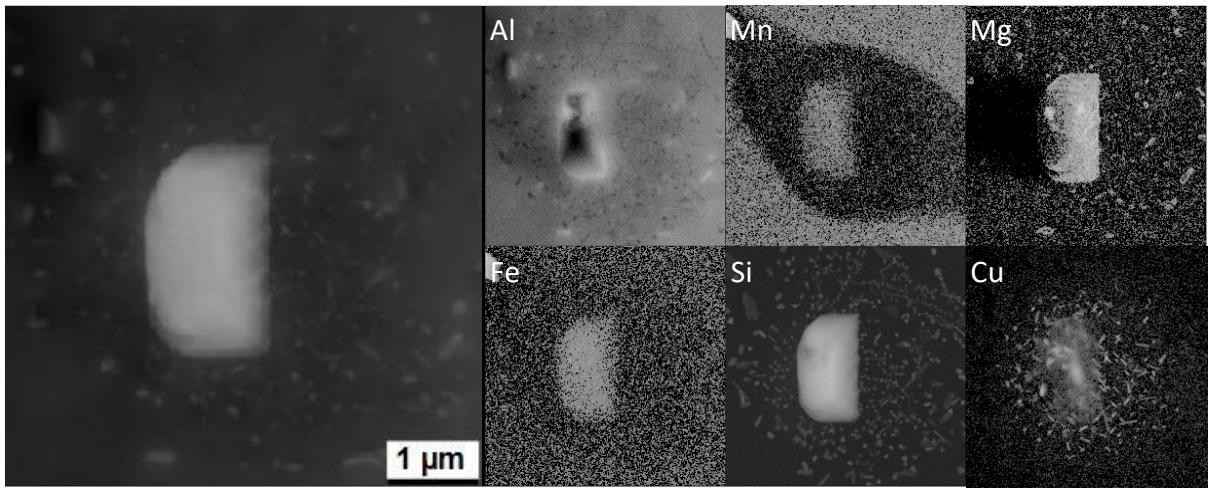

Fig. 7. STEM annular dark field images of the feature in Fig. 5b, and corresponding EDS maps of EN AW-3105 without Mg, heated to peak θ ′/Si (310 °C) at 0.01 K/s and subsequently water quenched to ambient temperature.

Fig. 5 shows TEM images of both alloys after heating to dedicated temperatures. These images show a detailed view of regions similar to those circled in the OLM images (Fig. 4). The Mg-containing alloy was heated at 0.01 K/s to 375 °C. It can be seen that several lath/rod-shaped particles have formed around a larger particle. These were identified by means of EDS (Fig. 6) as Mg-Si-Cu-containing lath/rods that accumulated around a large Si particle. The lath-shaped particles are likely related to the Mg-Si-Cu precursor phases. It can also be observed that the Si particle encloses a Mn,Fe-rich particle. This Mn,Fe-rich particle may be a primary phase acting as the nucleus for the Si particle. The TEM image in Fig. 7 shows the EN AW-3105 alloy without Mg after heating at 0.01 K/s to 310 °C. A large particle can be seen in the center of the image, with many smaller particles accumulated around it. These were identified by means of EDS (Fig. 7) as a large Si particle and smaller particles mostly consisting of Cu or Si. It is likely that the particles around the large one are θ′ and diamond Si, based on their respective shapes and compositions. Furthermore, it is interesting to note that the Mn concentration around the big Si particle is much lower than in the bulk material. This may suggest that a Mn-rich primary particle was close to this area and may have acted as a nucleus for the big Si particle (similar to Fig. 6), but that it probably fell out during the TEM sample preparation or was overlapped by the big Si particle.

The precipitation behavior of dispersoids was further investigated through TEM and EDS analysis of the precipitates. Fig. 8 shows TEM bright field images of EN AW-3105 with Mg heated just over the DSC d/e (240 °C) and δ-peak (375 °C), with a heating rate of 0.01 K/s. Small Mg-Si(-Cu) precursors have formed at the lowest temperature (240 °C). By increasing the temperature to 375 °C, these precursors have been dissolved and globular particles (few tens of nm in size) have precipitated. These small globular particles are presumably precipitated along previously existing Mg-Si(-Cu) precursor particles, because both are distributed along the [100] directions. As can be seen in Fig. 9, these were identified by means of EDS as Al, Mn, Fe, and Si phases and therefore are probably α-Al(Fe,Mn)Si dispersoids. This observation coincides with the observation of Lodgaard and Ryum [14], where they assumed that dispersoid precipitation proceeds along “u-phase” precipitates that have formed out of β′ precipitates due to Mn diffusion. In Fig. 8, as well as in Fig. 9, a single lath/rod-shaped particle can be observed, which consists of Mg and Si, and was analyzed by means of EDS in Fig. 9. We assume that this particle has remained and is just about to transform into dispersoids. This approach also means that the endothermic reaction F may not be a complete dissolution of β″/MgSiCu precursors, but rather a partial dissolution or transformation into dispersoids. With that in mind, the behavior of dispersoids in EN AW-3105 without Mg should differ from the Mg-containing alloy due to the lack of Mg-Si-Cu precursors acting as nucleation sites.

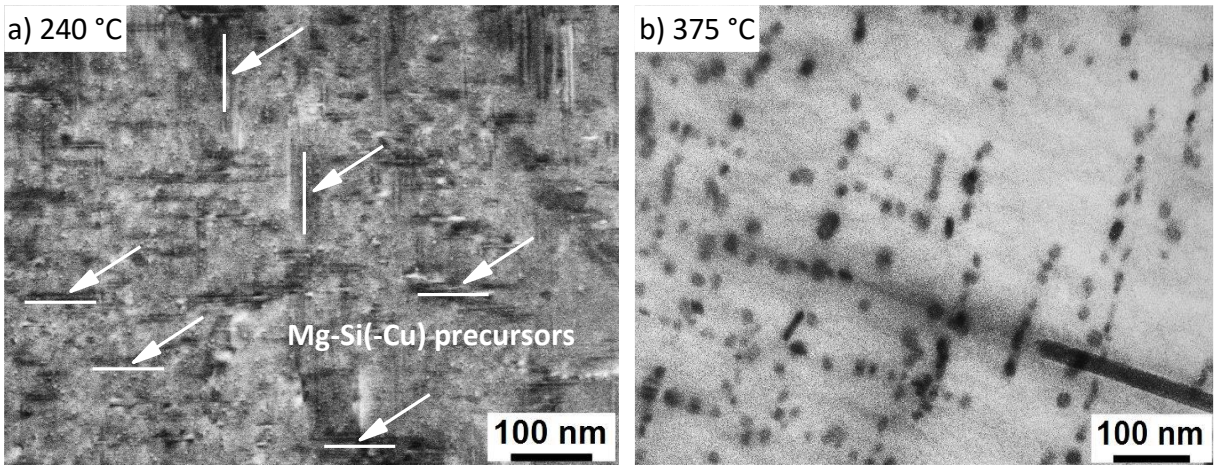

Fig. 8. TEM bright field images of EN AW-3105 with Mg heated to peak d/e (240 °C) in the [110] direction (a) and peak δ (375 °C) in [001] direction (b), respectively, at a heating rate 0.01 K/s and subsequently water quenched to ambient temperature.

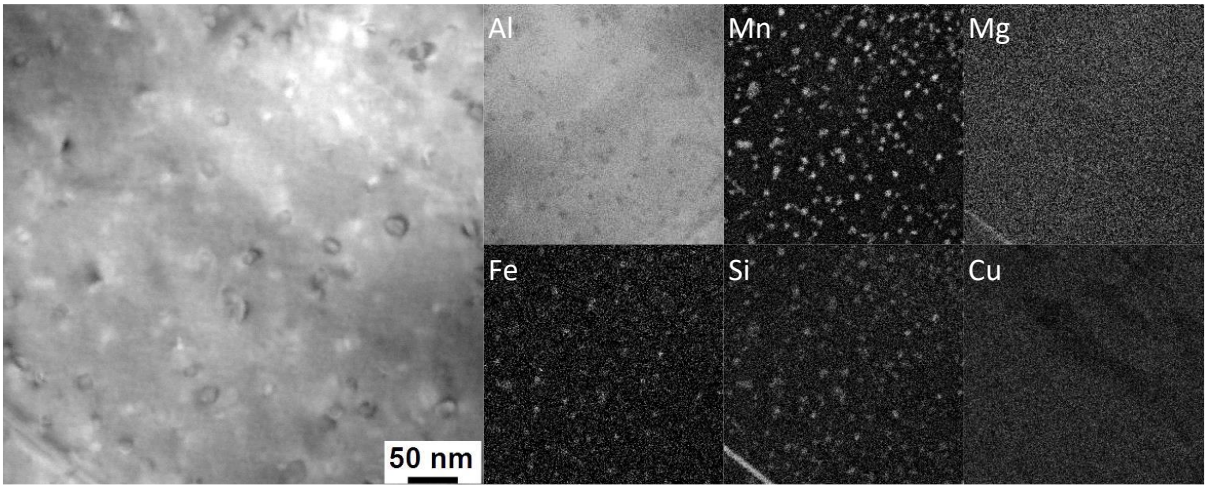

Fig. 9. STEM annular dark field image, with corresponding EDS maps, from the [001] zone axis of EN AW-3105 with Mg heated to 375 °C at 0.01 K/s and subsequently water quenched to ambient temperature.

3.3. Kinetics of dispersoid precipitation during heating with varying rates

Fig. 10 plots a range of DSC curves from the as-cast state of EN AW-3105 with and without Mg, with heating rates varying between 0.003 K/s and 2 K/s. The averaged DSC curves for different heating rates are shifted for clarity and are arranged in descending order of increasing heating rate. The change in EC has been plotted for the 1 K/s heating rate in Fig. 11. Corresponding zero-levels for the DSC curves are indicated as dotted lines.

It can be seen from Fig. 10 that the precipitation of dispersoids (δ-peak) depends not only on the temperature, but also on the heating rate. Its kinetics are expressed in the fact that an increasing heating rate leads to an increase in the δ-peak temperature. This temperature increase amounts to 65 K for EN AW-3105 with Mg (350 °C at 0.003 K/s to 415 °C at 0.1 K/s) and 100 K for EN AW-3105 without Mg (400 °C at 0.003 K/s to 500 °C at 2 K/s). This was to be expected due to the time dependency of diffusion processes such as dispersoid precipitation. However, it needs to be reiterated that different amount of endo- and exothermic signals may be superimposed on the DSC curve. DSC peak shifts (particularly in DSC heating curves) are thus difficult to evaluate. However, it is noted that at heating rates higher than 0.1 K/s, the

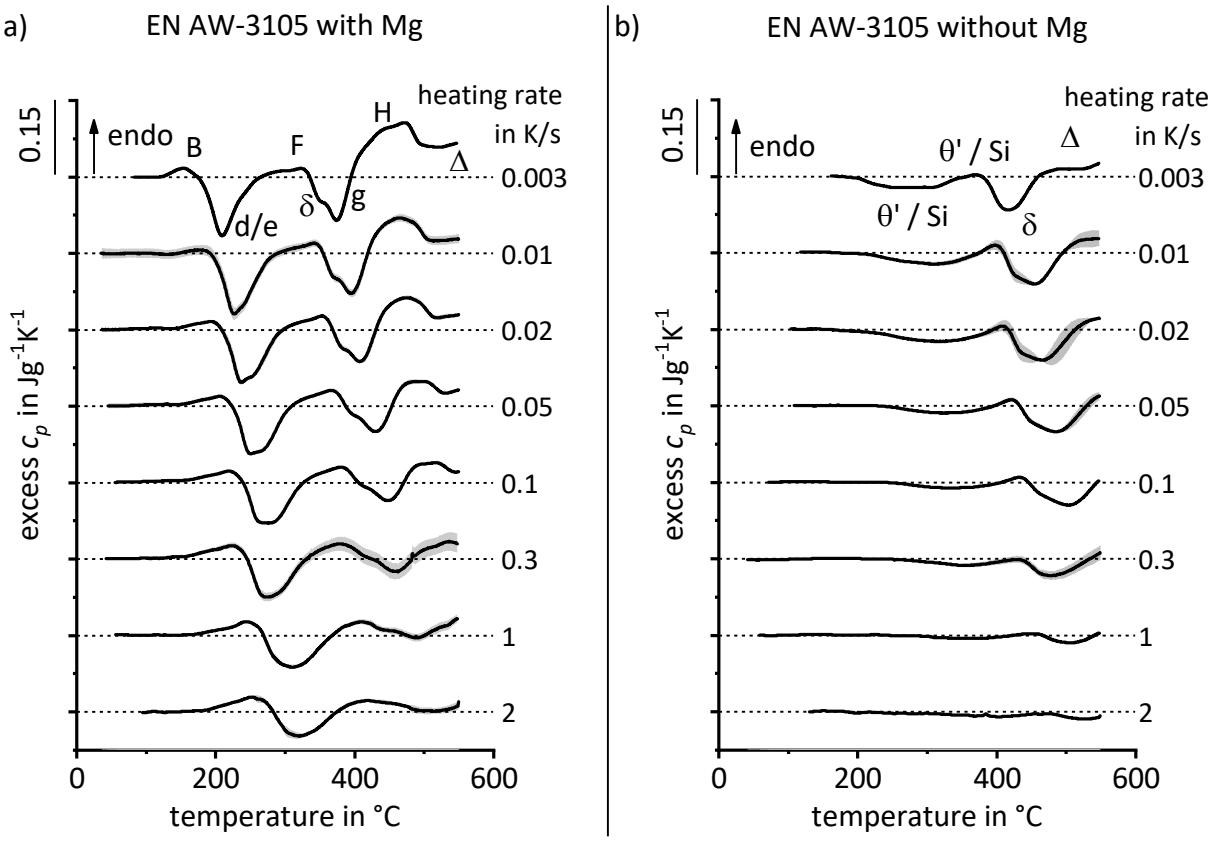

Fig. 10. Continuous zero-level DSC heating curves of EN AW-3105, with (a) and without Mg (b), at various heating rates.

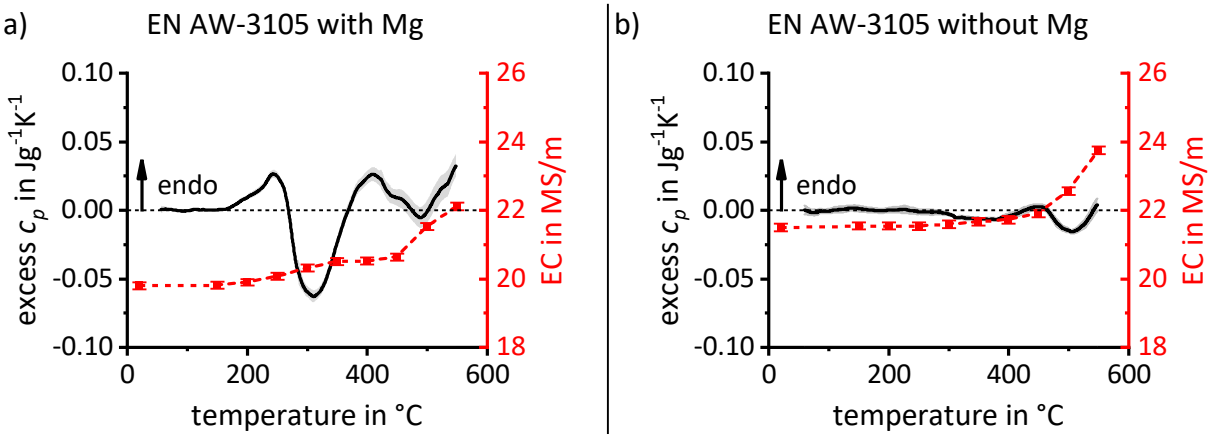

Fig. 11. Continuous zero-level DSC heating curves and electrical conductivity (EC) of EN AW-3105, with (a) and without Mg (b), for a linear heating rate of 1 K/s.

dispersoid precipitation of the Mg-containing alloy seems to be suppressed, and the DSC δ-peak vanishes, but it is also possible that the δ-peak may be substantially superimposed by peak F (dissolution of β″ and MgSiCu precursors, respectively).

Despite the challenges of DSC peak separation, it can also be seen from the EC measurements that the δ precipitation start temperature increases with increasing heating rate. At a heating rate of 0.01 K/s, the major increase in EC (associated with the dispersoid precipitation), of both alloys starts above 370 °C (Fig. 3). By increasing the heating rate to 1 K/s (Fig. 11), the dispersoid precipitation temperature is above 450 °C, which is again similar to the shoulder in the associated DSC curve of EN AW-3105 with Mg. However, the EC increases more

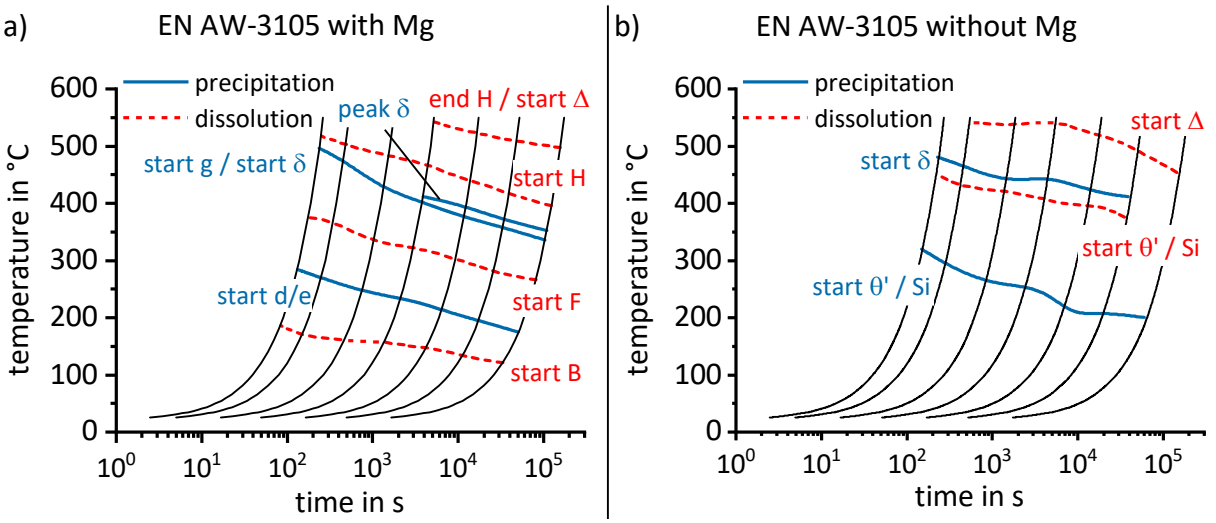

Fig. 12. Continuous heating dissolution diagrams of EN AW-3105 with (a) and without Mg (b). The curved lines represent the temperature profile of each heating experiment. The colored lines mark key precipitation (solid blue) and dissolution (dashed red) phases.

weakly at the higher heating rate, meaning that the volume fraction of the dispersoids is thus much smaller than the volume fraction at the slower heating rate. As previously discussed, the precipitation of dispersoids is a diffusion-based process that can be suppressed by higher heating rates, especially when one considers that Mn diffusion in Al is rather slow.

Fig. 12 shows the continuous heating dissolution diagrams of EN AW-3105 with and without Mg. The start temperatures of each separate phase were determined from the zero-crossing of the DSC curves of each heating rate. The precipitation start temperature of the dispersoids (δ) in the Mg-containing alloy cannot be explicitly determined by the zero-crossing due to the overlapping start of the precipitation reaction (g). Therefore, the peak temperature of the dispersoid reaction is also plotted in the diagram. Furthermore, the start of the dissolution reaction of the dispersoids (Δ) has been determined by the slope changes at high temperatures at the end of the reaction (H). It should be noted these temperatures are only an indication of the reaction temperatures due to the degree of overlap. In any case, it can be seen that the precipitation and dissolution start temperatures of each reaction increase with increasing heating rate.

3.4. Adapted heat treatment for fine dispersoid precipitation

As stated above, this work aims to identify adapted heat treatment parameters for Al-Mn-Fe-Si(-Mg) alloys that result in a high number density and small particle size of dispersoids. Such a fine dispersoid distribution should increase the strength, particularly for long-term applications at higher temperatures. Our approach is meant to enhance hardness/strength and electrical conductivity (EC). A conventional homogenization treatment might set other objectives, as for instance transforming the coarse primary Al(Mn,Fe)-Si intermetallic phase particles to variants less harmful on mechanical properties or processing. Nevertheless, if a strength increase and an additional increase in EC are intended, the first heat treatment after casting should be adapted. Based on the findings presented above, the adapted heat treatment parameters should fulfill the following criteria:

heating rate: The heating rate should be relatively slow to form a high volume fraction of Mg-Si(-Cu) precursors in a homogeneous distribution. These Mg-Si(-Cu) precursors later act as nuclei for dispersoid precipitation and ensure a homogenous distribution within the material. In alloys without Mg, a slow heating rate will probably lead to an even dispersoid distribution due to a uniform diffusion of Mn and Si.

temperature: The heat treatment temperature should be in the range between the dispersoid precipitation start temperature and beginning of growth dissolution. An appropriate temperature range can be estimated from slower DSC heating experiments.

One set of appropriate heat treatment parameters adapted for fine dispersoid precipitation was chosen as non-linear heating (adapted to billet heating in an industrial furnace to 400 °C, as explained in Fig. 1a). The isothermal treatment was conducted with soaking durations up to 100 h for the identification of reasonable soaking durations. A reasonable soaking duration for an application in electrical conduction systems is one that yields a high hardness combined with a good EC. The conventional homogenization temperature of 550 °C was used as a reference.

Fig. 13 shows the evolution of EC and hardness during isothermal heat treatment of as-cast EN AW-3105 with and without Mg. The adapted temperature of 400 °C is located about 30 K above the dispersoid formation start temperature (Fig. 3). One has to keep in mind that heating to 400 °C was conducted with a practical non-linear time-temperature profile. However, the influence of this heating path on the dispersoid formation is expected to be rather low compared to 0.01 K/s due to the similar total heating time.

The hardness of EN AW-3105 with Mg initially increases with time during isothermal heat treatment at 400 °C. The hardness reaches its maximum at 3 to 10 h and then decreases with prolonged soaking. The EC also increases with time, and continues to steadily increase, even after the hardness decreases. As mentioned before, the EC is heavily influenced by the concentration of Mn in solid solution, thus an increasing EC can be interpreted as an increase

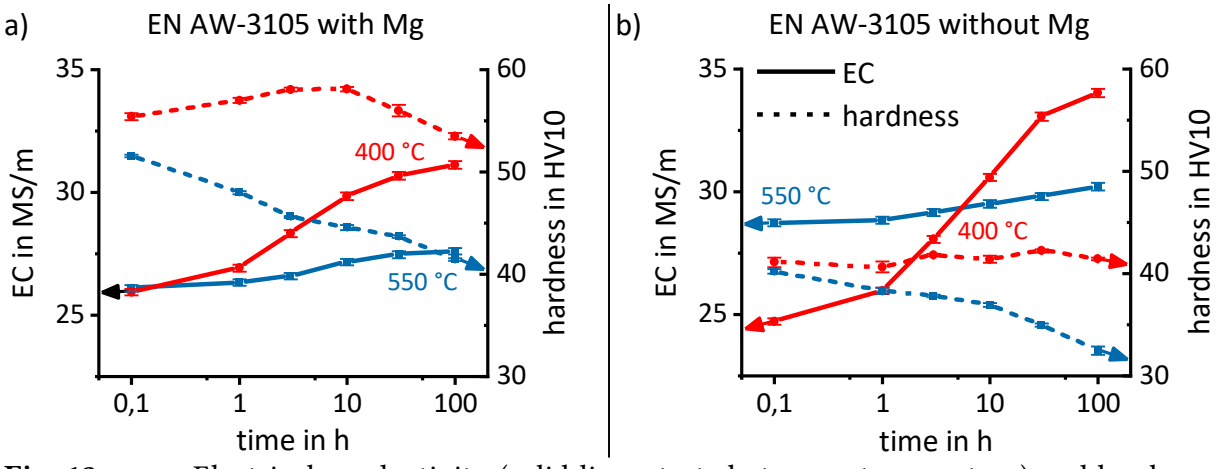

Fig. 13. Electrical conductivity (solid lines; tested at room temperature) and hardness evolution (dashed lines; tested at room temperature) measurements of EN AW-3105, with (a) and without Mg (b), during isothermal heat treatment at 400 (red) and 550 °C (blue), respectively.

in the volume fraction of dispersoids, in combination with coarsening of the dispersoids (see TEM results presented below). Although the hardness can be determined by multiple factors, i.e. nano-particles, grain size, dislocation density, etc., dispersoids are supposed to have the major influence on the hardness. The dispersoids presumably reach a critical particle radius leading to a hardness peak after 3 to 10 h of soaking at 400 °C. As long as the dispersoids are small, they pin dislocations effectively. In contrast, soaking of EN AW-3105 with Mg at 550 °C leads to a decreasing hardness although the EC is increasing. As can be concluded from the DSC and EC heating experiments, a heat treatment at 550 °C will lead to dissolution and growth of dispersoids and therefore decreases the contribution of dispersoids to the hardness. The simultaneous increase of EC likely is attributed to the dominance of the growth of dispersoids compared to their dissolution.

Although the EC of EN AW-3105 without Mg increases strongly with temperature, and therefore, the volume fraction of the dispersoids also increases, the hardness seems to remain unaffected during the isothermal heat treatment at 400 °C. In contrast to EN AW-3105 with Mg, the dispersoids are rather coarse due to the missing nucleation on β″/MgSiCu precursors, which is the primary reason for the small influence on hardness. It can thus be noted that hardness, as well as EC, can be improved by isothermal heat treatment at 400 °C and a reasonable soaking time compared to conventional homogenization parameters.

Fig. 14 shows OLM images of EN AW-3105 with and without Mg after different soaking times and at 400 °C. The term “directly quenched” is used for the condition after non-linear heating without any soaking time. It can be seen that several particles (Mg_2Si respectively Si / θ') have formed in addition to the primary particles within the aluminum matrix. By increasing the soaking time (100 h), most of these particles have either dissolved or become coarser, in accordance with the DSC results. At 400 °C, the β-Mg_2Si phase precipitates in EN AW-3105 with Mg and the Si / θ' phases in EN AW-3105 without Mg dissolve. Furthermore, it can be seen in EN AW-3105 without Mg that fine and evenly spread particles have formed within the aluminum matrix. These are the likely dispersoids that are expected to precipitate during the isothermal heat treatment. Precipitate free zones (PFZ) also observed around the primary particles, resulting from Mn depletion. The dispersoids visible in OLM are relative large, which explains their small influence on hardness. The dispersoids in the alloy without Mg further coarsen after 100 h at 400 °C (Fig. 14f). In contrast, dispersions can hardly be seen in the alloy with Mg due to their small size, even after 100 h at 400 °C (Fig. 14e).

Therefore, the dispersoid size and distribution was investigated by means of TEM for alloy EN AW-3105 with Mg after isothermal heat treatments at 400 °C for 10 h and 100 h (Fig. 15a and Fig. ***15***b, respectively). The images exhibit a large number of dispersoids (few tens of nm in size) within the material, with the dispersoids become coarser and less abundant with increasing soaking time. The two displayed sections indicate that the dispersoids are distributed more homogeneously after 100 h at 400 °C. The morphology of the dispersoids can be divided into two different shapes. The first type consists of randomly distributed polygonal plates, which may appear as either plates or needles based on the viewing angle [28]. The second type consists of cubic-shaped dispersoids, exhibiting an order of lines that may be the result of precipitation along the β″/MgSiCu precursors.

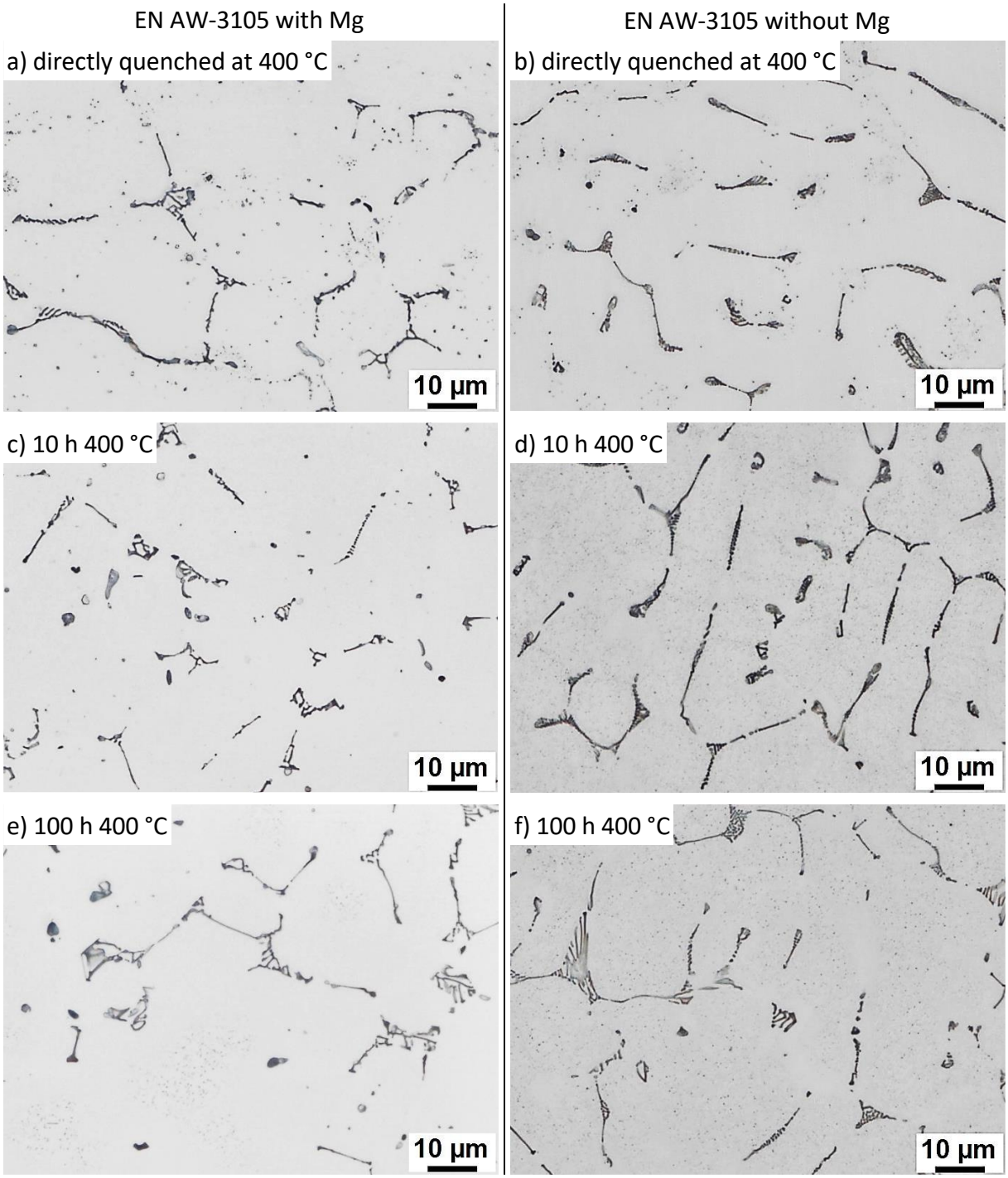

Fig. 14. OLM images of EN AW-3105 with (a,c,e) and without Mg (b,d,f), where the image sample was heated non-linear to 400 °C and then either directly quenched (a,b) or isothermally held for 10 h (c,d) and 100 h (e,f).

A quantitative analysis of dispersoid size, calculated from the TEM images, is presented in Fig. 16a, showing the relative frequency of particles with a certain Feret diameter. Fig. 16b presents the number density of particles after isothermal soaking at 400 °C for 10 and 100 h, respectively. The size distribution of the dispersoids shifts to larger particles when the isothermal soaking duration is increased, with the mean Feret diameter increasing from 44 to 56 nm. However, even after 100 h of heat treatment at 400 °C, the majority of the particles are <50 nm in size. The number density decreases with increasing soaking time from 531 ± 112

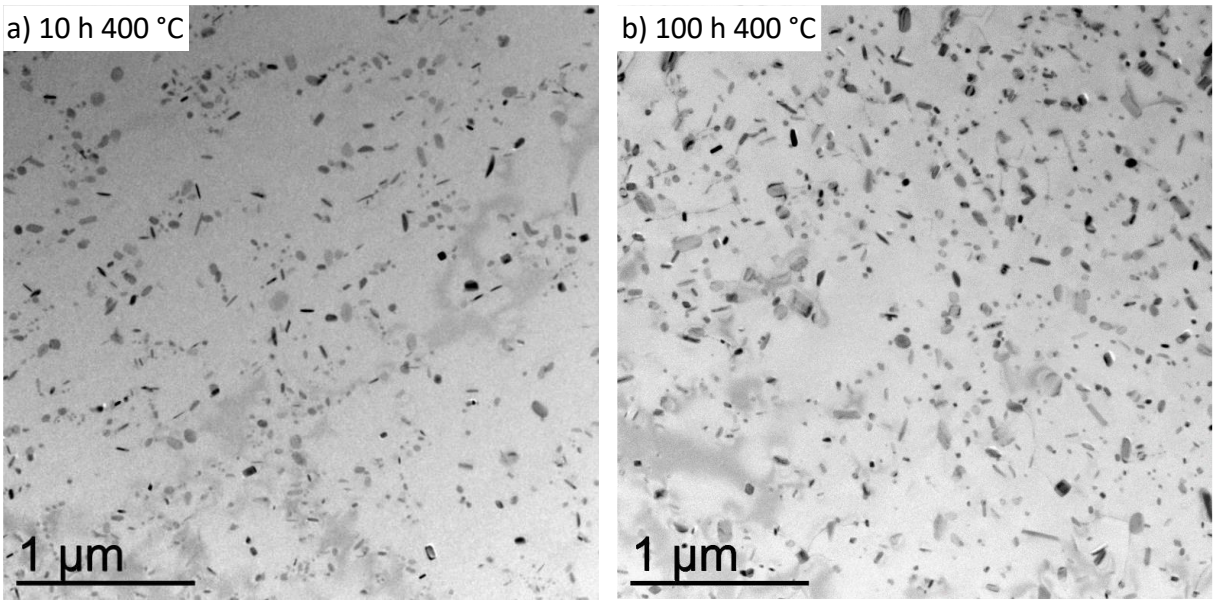

Fig. 15. TEM bright field image of EN AW-3105, heated non-linearly to 400 °C and isothermally held for 10 h (a) and 100 h (b).

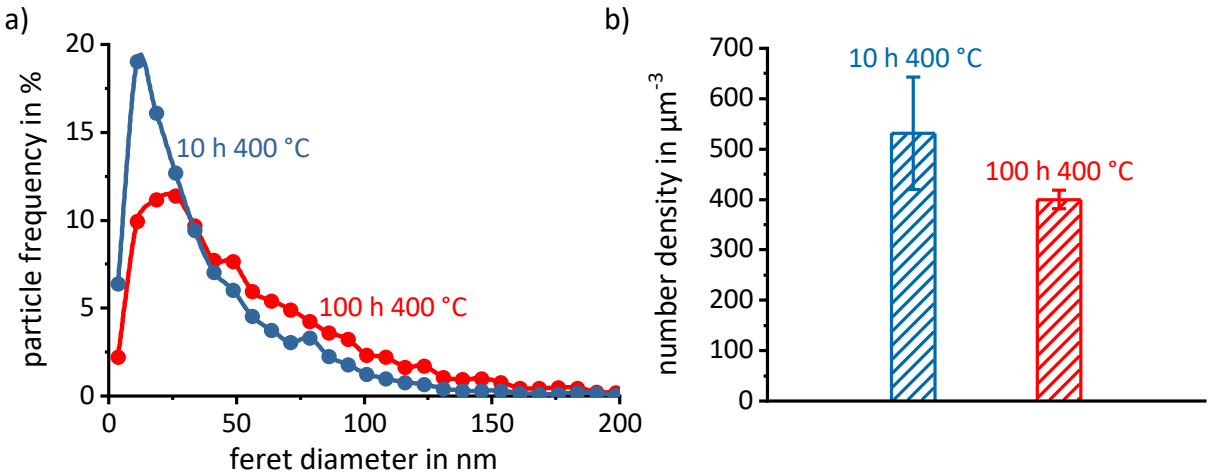

Fig. 16. Dispersoid size distribution (a) and number density (b) in EN AW-3105 with Mg, heated non-linearly to 400 °C and isothermally held for 10 h (blue) and 100 h (red).

to 400 ± 19 µm^{-3}. Both effects are likely due to Oswald ripening. The standard deviation decreases significantly with increasing soaking time, indicating that a more even distribution of dispersoids (only with respect to their number density) is achieved.

Standard homogenization treatments at 550 °C show that both alloys generally exhibit a steady decline in hardness with increasing soaking time (Fig. 13) due to the coarsening of dispersoids. Alloy EN AW-3105 with Mg thus shows the promising properties of high hardness and good EC after isothermal soaking at 400 °C for 10 h.

4. Summary

The precipitation behavior of dispersoids in Direct Chill casted aluminum alloy EN AW-3105 with and without Mg has been investigated. In situ Differential Scanning Calorimetry (DSC) experiments show a clear superposition of different precipitation and dissolution reactions. For the first time, the precipitation start temperature for dispersoids was determined by in situ DSC and found to be ~370 °C for a heating rate of 0.01 K/s. Increasing the heating rate

yielded an increase in the precipitation start temperature and suppressed dispersoid precipitation. As novelty, it is thus suggested that the homogenization temperature can be reduced from 550 °C to 400 °C to achieve the optimal dispersoid strengthening effect in combination with a substantial increase in electrical conductivity. Isothermal experiments at 400 °C have shown significant improvement in the hardness (up to 30 %) and electrical conductivity (up to 10 % compared to a conventional homogenization treatment). The latter indicates an increase in number density & volume fraction of dispersoids. This was confirmed by Transmission Electron Microscopy. By the newly suggested (homogenization) treatment, alloy EN AW-3105 with Mg yielded its highest hardness of 58 HV10 after 3 to 10 h of heating at 400 °C. Our results confirm the important role of Mg in this type of alloy, as Mg-Si precursor phases seem to act as nucleation sites for dispersoid precipitation. Therefore, the presence of Mg potentially is leading to an increased number density of fine, evenly distributed dispersoids.

Acknowledgements

The authors gratefully acknowledge Hydro Aluminium R&D, Bonn, Germany, for providing the materials used in this study. This work was supported by the Research Council of Norway (RCN) (grant number 221714) and the German Federal Ministry of Education and Research (BMBF) (project 03EK3538A). The experimental TEM work was partially carried out on the NORTEM instrument JEOL JEM-2100F, TEM Gemini Center, NTNU, Norway (grant number 197405).

References

[1] M. Dehmas, E. Aeby-Gautier, P. Archambault, M. Serrière, Interaction Between Eutectic Intermetallic Particles and Dispersoids in the 3003 Aluminum Alloy During Homogenization Treatments, Metall. Mater. Trans. A 44(2) (2013) 1059–1073.

[2] D.T.L. Alexander, A.L. Greer, Solid-state intermetallic phase tranformations in 3XXX aluminium alloys, Acta Mater. 50(10) (2002) 2571–2583.

[3] A. Håkonsen, D. Mortensen, S. Benum, T. Pettersen, T. Furu, Modelling the Metallurgical Reactions during Homogenisation of an AA3103 Alloy, in: J.F. Grandfield, D.G. Eskin (Eds.), Essential Readings in Light Metals, John Wiley & Sons, Hoboken, NJ, USA, 2013, pp. 1028–1035.

[4] Y.J. Li, L. Arnberg, A eutectoid phase transformation for the primary intermetallic particle from Alm(Fe,Mn) to Al3(Fe,Mn) in AA5182 alloy, Acta Mater. 52(10) (2004) 2945–2952.

[5] Y. Zhang, Z. Zhang, R.E. Sanders, Q. Liu, Study of the phase transformation from (Fe, Mn)Al_6 TO α-Al_{12}(Fe, Mn)$_3$Si in AA3104 aluminum alloy during homogenization, Acta Metall. Sin. 48(3) (2012) 351–356.

[6] M. Dehmas, P. Weisbecker, G. Geandier, P. Archambault, E. Aeby-Gautier, Experimental study of phase transformations in 3003 aluminium alloys during heating by in situ high energy X-ray synchrotron radiation, J. Alloys Compd. 400(1–2) (2005) 116–124.

[7] D.T.L. Alexander, R.G. Hamerton, H. Cama, A.L. Greer, Investigating the Alpha Transformation - A Solid-State Phase Change of Dispersed Intermetallic Particles from an Al 6 (Fe,Mn) Phase to an α-Al-(Fe,Mn)-Si Phase, in: J.F. Grandfield, D.G. Eskin (Eds.), Essential Readings in Light Metals, John Wiley & Sons, Hoboken, NJ, USA, 2013, p. 1013–1020.

[8] Y.J. Li, L. Arnberg, Quantitative study on the precipitation behavior of dispersoids in DC-cast AA3003 alloy during heating and homogenization, Acta Mater. 51(12) (2003) 3415–3428.
[9] Y.J. Li, A.M.F. Muggerud, A. Olsen, T. Furu, Precipitation of partially coherent α-Al(Mn,Fe)Si dispersoids and their strengthening effect in AA 3003 alloy, Acta Mater. 60(3) (2012) 1004–1014.
[10] Y.F. Cheng, V. Hansen, J. Gj, L.R. Wallenberg, TEM study of the early stages of the precipitation process in strip-cast Al3003 alloys, J. Mater. Res. 7(12) (1992) 3235–41.
[11] K. Liu, X.-G. Chen, Evolution of Intermetallics, Dispersoids, and Elevated Temperature Properties at Various Fe Contents in Al-Mn-Mg 3004 Alloys, Metall. Mater. Trans. B 47(6) (2016) 3291–3300.
[12] R. Hu, T.Ogura, H. Tezuka, T. Sato, Q. Liu, Dispersoid formation and recrystallization behavior in an Al-Mg-Si-Mn alloy, J. Mater. Sci. Technol. 26(3) (2010) 237–243.
[13] A.R. Eivani, H. Ahmed, J. Zhou, J. Duszczyk, Correlation between Electrical Resistivity, Particle Dissolution, Precipitation of Dispersoids, and Recrystallization Behavior of AA7020 Aluminum Alloy, Metall. Mater. Trans. A 40(10) (2009) 2435–2446.
[14] L. Lodgaard, N. Ryum, Precipitation of dispersoids containing Mn and/or Cr in Al–Mg–Si alloys, Mater. Sci. Eng. A 283(1-2) (2000) 144–152.
[15] Y.J. Li, W.Z. Zhang, K. Marthinsen, Precipitation crystallography of plate-shaped Al 6(Mn,Fe) dispersoids in AA5182 alloy, Acta Mater. 60(17) (2012) 5963–5974.
[16] P.N. Anyalebechi, Investigation of the effects of as-cast microstructure and temperature on the response of aluminum alloy 3004 ingots to homogenization, in: M.E. Schlesinger (Ed.), EPD Congress 2005, TMS (The Minerals, Metals, and Materials Society), 2005, pp. 519–538.
[17] G.A. Edwards, K. Stiller, G.L. Dunlop, M.J. Couper, The precipitation sequence in Al-Mg-Si alloys, Acta Mater. 46(11) (1998) 3893–3904.
[18] R.H. Kemsies, B. Milkereit, O. Kessler, T. Fuhrmann, S. Schlegel, F. Plonus, S.P. Miller-Jupp, J. Hirsch, Effect of Dispersoids on Long-Term Stable Electrical Aluminium Connections, Mater. Sci. For. 877 (2016) 409–415.
[19] A.M.F. Muggerud, E.A. Mørtsell, Y.J. Li, R. Holmestad, Dispersoid strengthening in AA3xxx alloys with varying Mn and Si content during annealing at low temperatures, Mater. Sci. Eng. A 567 (2013) 21–28.
[20] R.V. Tilak, J.G. Morris, Studies of the effect of thermomechanical treatments on the supersaturation content of strip-cast aluminum alloy 3004, Mater. Sci. Eng. 73 (1985) 139–150.
[21] K. Liu, X.-G. Chen, Development of Al–Mn–Mg 3004 alloy for applications at elevated temperature via dispersoid strengthening, Mater. Des. 84 (2015) 340–350.
[22] N.J. Luiggi, Isothermal precipitation of commercial 3003 Al alloys studied by thermoelectric power, Metall. Mater. Trans. B 28(1) (1997) 125–133.
[23] J. Osten, B. Milkereit, C. Schick, O. Kessler, Dissolution and precipitation behaviour during continuous heating of Al-Mg-Si alloys in a wide range of heating rates: Materials, Mater. 8(5) (2015) 2830–2848.
[24] L.R. Feret, La grosseur des grains des matières pulvérulentes, Premières Communications de la Nouvelle Association Internationale pour l’ Essai des Matériaux, Groupe D, 1931, pp. 428–436.

[25] D. Altenpohl, Aluminium und Aluminiumlegierungen, Springer-Verlag, Berlin-Heidelberg-New York, 1965.
[26] Y. Ohmori, L.C. Doan, Y. Matsuura, S. Kobayashi, K. Nakai, Morphology and crystallography of β-Mg2Si precipitation in Al–Mg–Si alloys, Mater. Trans. 42(12) (2001) 2576–2583.
[27] C. Barbosa, J.M.A. Rebello, O. Acselrad, J. Dille, J.-L. Delplancke, Identification of Precipitates in 6013 Aluminum Alloy (Al–Mg–Si–Cu), Z. Metallk. 93(3) (2002) 208–211.
[28] D.L. Sun, S.B. Kang, H.S. Koo, Characteristics of morphology and crystal structure of α-phase in two Al-Mn-Mg alloys, Mater. Chem. and Phys. 63(1) (2000) 37–43.